Design of Ionic Liquid Crystals Enabled by [2]Rotaxane Structure Formation

Journal:	*Molecular Systems Design & Engineering*
Manuscript ID	ME-ART-02-2024-000034.R1
Article Type:	Paper
Date Submitted by the Author:	12-May-2024
Complete List of Authors:	Washino, Gosuke; Tokyo Institute of Technology Kajitani, Takashi; Tokyo Institute of Technology Nishimura, Suzushi; Tokyo Institute of Technology Shishido, Atsushi; Tokyo Institute of Technology

This paper reports a new molecular design concept for liquid crystalline (LC) molecules utilizing rotaxane structure formation.

In this molecular design, an ionic axle molecule threads through a ring molecule with flexible tails, forming a [2]rotaxane. Although neither the single axle nor the ring has any LC properties, the resulting [2]rotaxane exhibited thermotropic LC properties due to the integration of the mesogen core and flexible tails via rotaxane structure. In addition to diversifying the design approach for LC molecules, this molecular design concept enables the creation of highly functional materials that cross the rotaxane molecule with the ordered order of LCs.

Desired system functionality would include anisotropic rheology or mechanical properties, in which the higher-order structure of the LC controls the dynamic motions of rings in a rotaxane.

Future applications aim to create dynamic supramolecular LC molecules by developing this molecular design into pseudo-rotaxanes. This would create stimuli-responsive LC materials involving the reversible dissociation and aggregation of pseudo-rotaxane structure.

ARTICLE

Design of Ionic Liquid Crystals Enabled by [2]Rotaxane Structure Formation

Received 00th January 20xx,
Accepted 00th January 20xx

DOI: 10.1039/x0xx00000x

Gosuke Washino[a], Takashi Kajitani[b], Suzushi Nishimura[c], and Atsushi Shishido*[a,d]

We report a new synthetic concept for converting isotropic ionic molecules into thermotropic ionic liquid crystals by forming [2]rotaxane structures. Our results demonstrate the synthesis of liquid-crystalline (LC) rotaxane from an ionic axle molecule as a mesogen core and a molecular ring as flexible tails, neither of which possess LC properties. The obtained [2]rotaxane exhibited an interdigitated smectic A phase at around 140 °C. A simple mixture of the axle and ring, which cannot form a rotaxane structure, did not show LC. A [2]rotaxane compound having a ring with shorter flexible tails did not show an LC phase, either. These comparisons revealed that the integration of the mesogen core and sufficient length flexible tails into one molecule via rotaxane structure enables the emergence of LC nature. Our results prove that rotaxane structure serves as a connection to spatially introduce flexible tails into the mesogen core, pioneering a new approach to LC molecular design.

Introduction

Ionic molecules[1–3] exhibit ionic conductivity[4] or redox[5,6] properties through ion–ion interactions or ion transfer. Ionic molecules showing a liquid-crystalline (LC) phase are called ionic LCs (iLCs)[7–10], which possess both ionic and LC properties; ionic molecules can be arranged with the higher-order structure, leading to the improvement of material properties specific to ionic molecules on a macro scale[11,12]. Numerous LC molecules have been reported, and their molecular design strategies have been systematized[13–18]. For thermotropic LC molecules, a basic design concept is to introduce a mesogen core and a flexible tail into a single molecule[19]. Another LC molecular design is to induce phase separation by adjusting the balance of intramolecular hydrophilicity and hydrophobicity[20]. Regarding LC expression, iLCs have superior design versatility because counter ions[21,22] can be taken advantage of in addition to conventional non-ionic design methods[23]. In particular, rigid organic cations, including viologen[24,25] and pyridinium[26], play a central role in the design of iLCs.

When combined with electron-rich donors, rigid cations also serve as acceptors to form charge transfer (CT)[27,28] complexes. The intramolecular donor–acceptor interactions allow for molecular self-assembly, leading to supramolecular systems[29]. For the synthesis of mechanically interlocked molecules (MIMs)[30–33], known for rotaxanes[34–37] and catenanes[38,39], donor–acceptor interactions due to rigid cations are widely employed[40,41]. Mixing rigid cationic molecular axles, such as viologen or pyridine-ethane derivatives, with electron-rich rings like crown ethers yields a threading structure: pseudo-rotaxane[42,43]. Capping both ends of the axle in pseudo-rotaxane with bulky substituents provides rotaxane[40,44,45]. Thus, rigid cations are important molecular components for both iLC and rotaxane design.

However, very few syntheses of LC molecules with rotaxane structure have been reported[46–48]. In 2006, Kato and Stoddart first reported an LC [2]rotaxane based on a cationic ring and electron-rich axle with dendric mesogenic stoppers[16]. Utilizing the dual roles of cations[24] in the different research fields, Loeb and Eichhorn[49] reported [2]rotaxanes exhibiting thermotropic LC phases where 1,2-bis(4,4'-bipyridinium)ethane[42] core with flexible tails at both ends threads a dibenzo-24-crown-8 (DB24C8) ring. In their design, the ionic axles alone, consisting of both a mesogen core and flexible tails, show a soft crystal but no LC phase without a ring. The DB24C8 on the axle thermally stabilized the axle by shielding the axles' interaction, allowing the resulting [2]rotaxane to express a stable LC phase. The stability of iLC can be also tuned by the selection of counter ions depending on their size and hardness[50]. Considering functions previously reported on the iLCs[51] and rotaxanes[52–54], their combination is expected to create unique, synergetic functions. However, the synthesis examples remain limited to the concept that relies on the connection of a mesogenic axle with flexible tails and a ring. This approach requires the design of complex axle structures containing flexible tails and a mesogen core, leading to increased synthetic burden and limitation of molecular design freedom. This could hinder the efficient

[a] Laboratory for Chemistry and Life Science, Institute of Innovative Research, Tokyo Institute of Technology, 4259 Nagatsuta, Midori-ku, Yokohama 226-8501, Japan.
[b] Open Facility Center, Tokyo Institute of Technology, 4259 Nagatsuta, Midori-ku, Yokohama 226-8501, Japan.
[c] School of Materials and Chemical Technology, Tokyo Institute of Technology, 4259 Nagatsuta, Midori-ku, Yokohama 226-8501, Japan.
[d] Research Center for Autonomous Systems Materialogy, Institute of Innovative Research, Tokyo Institute of Technology, 4259 Nagatsuta, Midori-ku, Yokohama 226-8501, Japan.

†Electronic Supplementary Information (ESI) available: [details of any supplementary information available should be included here]. See DOI: 10.1039/x0xx00000x

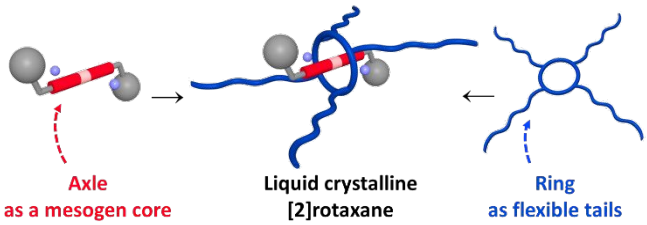

Fig. 1 Illustration of liquid-crystalline [2]rotaxane by the combination of an axle as a mesogen core and a ring as flexible tails

design of functional iLCs and rotaxanes; thus, pioneering a new synthetic concept for LC rotaxanes is crucial for the growth of the field.

Here, we report a novel approach to designing iLCs utilizing the rotaxane structure formation. We synthesized a [2]rotaxane with an axle molecule as a mesogen core and a ring molecule as only flexible tails (Fig. 1). The resultant [2]rotaxane showed a thermotropic LC phase with a smectic layer structure; by contrast, neither the axle nor ring had LC properties. The evaluation of a series of axle, ring, and rotaxane compounds confirmed that the rotaxane integrated with the axle with a mesogen core and ring with flexible tails enables the LC emergence. Our iLC synthesis concept utilizing rotaxane formation will expand the versatility of the iLC molecular design approach, leading to a further greater degree of molecular design freedom.

Results and Discussion

Synthesis of Liquid-Crystalline Rotaxane

To demonstrate our design concept, we synthesized an iLC [2]rotaxane **Rtx12** (Fig. 2a) consisting of a molecular ring **R12** (Fig. 2c) with four 12-carbon alkyl chains on a dibenzo-24-Crown-8 (DB24C8) ring and an ionic axle molecule **A1** (Fig. 2b) composed of a 1,2-bis(4,4'-bipyridinium)ethane (BDPE) core (See Scheme S1 for synthetic route). In this study, we selected bis(trifluoromethyl sulfonyl)imide (NTf_2) as the counter anion to lower the phase transition temperature[50]. **R12** was prepared by reacting a derivative of DB24C8 with four bromomethyl groups[55] and 4-(dodecyloxy)phenol[56], introducing four C12 chains via phenyl ether groups into DB24C8. When adding **R12** to a solution of BDPE, a precursor of A1 without *tert*-butyl stoppers in CH_3NO_2:$CHCl_3$ (2:1, v/v), the solution turned orange, indicating pseudo-rotaxane formation. To the reaction, 9 equivalents of 4-tert-benzyl bromide were added and stirred at room temperature for 5 days to cap both ends of BDPE with a bulky tert-benzyl group, confining **R12** on **A1**. An orange solid obtained after purification was characterized as **Rtx12** by solid-state UV–vis, nuclear magnetic resonance (NMR), and high-resolution mass spectroscopy (HRMS) (Fig. S19–S23). In the collected UV-vis spectra, we observed the presence of a new absorption band centred at 422 nm in **Rtx12**, which was not observed in either single **A1** or **R12**. This is attributed to the formation of a stable CT complex between the electron-poor BDPE core of **A1** and electron-rich benzenic moieties of **R12** in **Rtx12**. On the other hand, an equimolar mixture of **A1** and **R12** did not show such a clear band as **Rtx12**. This result matches the fact that BDPE before capping with the *tert*-butyl group can form a threatening structure with the DB24C8 ring but cannot after capping due to steric hindrance. In the ^{1}H NMR spectrum, every proton constituting **Rtx12** was detected at appropriate chemical shifts with good integration ratios. This indicates that **Rtx12** was successfully synthesized and isolated in a form consisting of a 1:1 equivalent of **A1** and **R12**. In addition, to confirm the formation of rotaxane structure, we tracked the chemical shift of the axle **A1** in three different states: **A1** alone, in **Rtx12**, and a mixture with **R12** (Fig. 2d). In **Rtx12**, a set of peak shifts of the **A1**-derived proton signal was observed, *e.g.*, the α-pyridinium proton *a* and the ethylene proton ***i*** displayed downfield shifts compared with bare **A1** ($\Delta\delta$ = 0.35 and 0.40, respectively; see details in Table S1). This means the BDPE core of **A1** receives strong electron donation from **R12**, increasing the effective electron density. In fact, the observed **A1**-derived

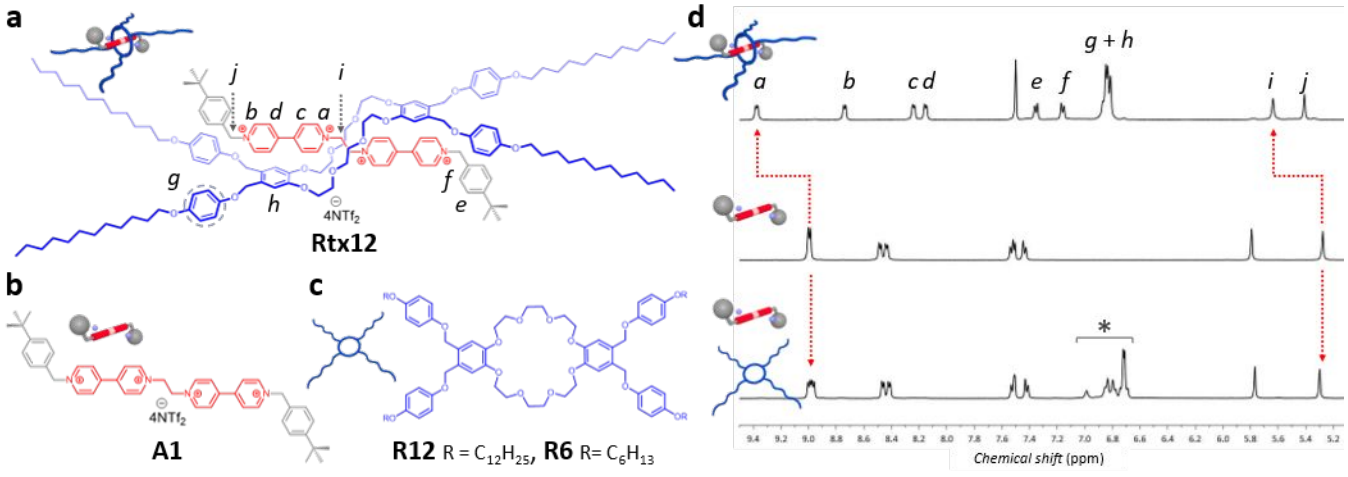

Fig. 2 Chemical structure of a) **Rtx12**, b) **A1**, and c) **R12/R6**. d) Partial ^{1}H NMR (CD_3CN/$CDCl_3$, 1:1, v/v, 400 MHz) of **Rtx12** (top), **A1** (middle), and 1:1 mixture of **A1** and **R12**(bottom). *Denotes protons of **R12**.

chemical shifts in **Rtx12** are consistent with those reported for [2]rotaxane (**A1** ⊃ DB24C8)[44] (Table S1), supporting that **Rtx12** has [2]rotaxane structure where **R12** sits on the BDPE core[42] of **A1**. On the other hand, when mixed with equimolar **R12**, **A1** proton signals overlapped with those of **R12** without showing any significant peak shifts. Additionally, the equimolar mixture showed no significant absorbance in the solid-state UV–vis spectra (Fig. S23). This means that the mixture of **A1** and **R12** forms no rotaxane structure, and **R12** cannot move beyond the *tert*-butyl group. Furthermore, the ^{1}H-^{1}H NOESY NMR result showed the correlations between protons of the ionic core of **A1** and those of the benzene moieties on the ring rim of **R12**, suggesting that **R12** sits on the BDPE moiety of **A1**. Finally, ESI-HRMS detected [**Rtx12** + 2NTf$_2$]$^{2+}$ at *m/z* = 1402.1742 for, ($C_{148}H_{202}F_{12}N_6O_{24}S_4$, calc. 1402.1742; relative error 1.3 ppm) confirming the presence of **Rtx12**. All our analytical results consistently supported the successful synthesis of **Rtx12**.

Phase Transition Behaviour of Rtx12

The phase transition behavior including LC properties of **Rtx12** was characterized by differential scanning calorimetry (DSC, Fig S33), temperature-dependent X-ray diffraction (VT-XRD, Fig 3a), and polarized optical microscopy (POM, Fig 3b). In the DSC thermogram at the rate of 10 °C/min, no valid peaks were found in the cooling process. The following heating process showed multiple small exothermic peaks and then two broad endothermic peaks at 140 and 170 °C, respectively. In POM observation, when heated to 170 °C, **Rtx12** displayed a fluidic dark field showing an isotropic phase. Upon cooling from the isotropic phase, batonnets/fan-shape textures having clear fluidity appeared around 140 °C (Fig. 3b), confirming that **Rtx12** is a thermotropic LC. While further cooling down to 20 °C, this texture gradually lost its fluidity and was immobilized. **Rtx12** recovered the original flowable batonnets/fan-shape textures above 140 °C in the following heating process. Then, it transitioned to the isotropic phase again at 170 °C. Based on the DSC and XRD results, we assign the phase transition temperatures of **Rtx12** as follows. During the cooling process, **Rtx12** do not show a clear first-order phase transition, but a gradual isotropic–crystalline phase transition, showing an LC phase between them. In the heating process, **Rtx12** exhibits partial crystallization below 125 °C, a crystalline–LC phase transition at 140 °C, and then an LC–isotropic phase transition at 170 °C. To characterize the type of LC phase and its detailed phase transition behaviour, we conducted VT-XRD scans of **Rtx12** during the cooling process from 150 to 25 °C by every 5 °C under an argon atmosphere (Fig. 3a). At 150 °C, **Rtx12** exhibited strong diffraction peaks at 2ϑ = 2.38 and 4.77°, corresponding to *d*-spacing of 37.1 and 18.5 Å, respectively (1:1/2 peak ratio). A halo peak centred at 2ϑ = 17.1°, fulfilling typical smectic phase features. Considering the XRD results with the battonets texture observed in the POM together, we conclude that **Rtx12** exhibits a smectic A (SmA) phase. At 130 °C during the cooling process, several small diffraction peaks appeared in the broad range of 2ϑ = 6–25° in addition to those originating from the SmA phase, confirming the transition of **Rtx12** from the SmA phase to the crystalline phase while maintaining a layered structure: soft crystal[49]. Subsequent cooling to 25 °C resulted in only a slight strengthening of the crystal-derived diffraction, and no significant structural changes were found in the X-ray diffraction. For further discussion on the phase transition behaviour upon cooling, we plotted the interlayer distance *d* calculated from 2ϑ corresponding to the first-order diffraction peaks in the XRD scans at each temperature (Fig. 3c). The plots clearly showed discontinuous change in *d* value at 130 °C, supporting phase transition from the SmA phase to the crystalline phase indicated by a change in XRD pattern. On further cooling, the *d* value significantly dropped again at 90 °C, but at the lower temperature, it was relatively stable overall. The XRD patterns of **Rtx12** at 90 and 25 °C were identical to each other, whereas that of at 130 °C showed some difference (Fig. S34). Furthermore, POM images in the crystalline phase exhibited no significant changes, either. Taking these results into account, a crystalline–crystalline phase transition exists at 90 °C. Then, in the XRD scanning upon heating from 25 to 150 °C by every 5 °C, a wide range of small diffraction peaks derived from crystalline **Rtx12** disappeared at 145 °C, indicating a crystalline to SmA phase transition. Together with the broad endothermic peak centred at 140 °C in DSC and textures observed by POM, we conclude that **Rtx12** undergoes the crystalline–SmA phase transition at 140 °C upon heating. Further heating showed that **Rtx12** exhibited an isotropic phase at 170 °C, as indicated by POM and DSC results.

To discuss the thermal stability of **Rtx12**, we collected **Rtx12** after DSC measurements at different maximum temperatures.

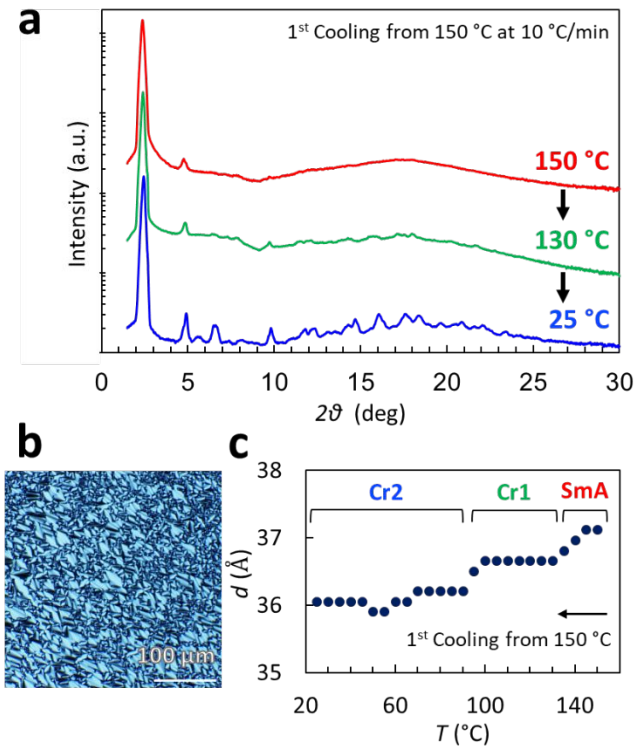

Fig. 3 Phase transitions of **Rtx12** upon cooling. a) XRD pattern of **Rtx12**. b) POM image of **Rtx12** at 150 °C. c) Layer distance *d* of **Rtx12** calculated from XRD data through cooling process.

Then we compared their ^{1}H NMR spectra with those before heating (Fig. S35). No change was observed in **Rtx12** heated at 175 °C. However, unexpected broadening and emergence of small peaks were detected for **Rtx12** heated up to 190 °C. This means **RTx12** can maintain its molecular structure below 175 °C but involves decomposition risk above 175 °C. Indeed, endothermic peaks of **Rtx12** in the DSC heating process disappeared once heated to 190 °C. Moreover, in the VT-XRD measurement at 175 °C, Rtx12 showed a diffraction pattern indicating an isotropic phase, but the decomposition was detected after the cooling process, suggesting that the isotropic phase would be thermally unstable. The phase transition behaviour of **Rtx12** is summarized in Fig. 4.

Finally, to understand the molecular arrangements of **Rtx12** in the SmA layered structure, we performed DFT calculations (B3LYP, 6-31g(d.p)) of the stable structure of **Rtx12** (Fig. S36). In the calculated structure, the ring molecule sits on the axle with an S-shaped conformation, which allows the flexible tails on the ring to stabilize in a similar direction as the mesogen core of the axle. The polarized infrared (IR) absorption spectra of the uniaxially oriented **Rtx12** (Fig. S38) prepared by share application in the SmA phase state supported this result; Both the aliphatic alkyl moieties of the ring and the cationic nitrogen-carbon moieties of the axle were aligned parallel to the shear direction. The total molecular length (*L*) of **Rtx12** estimated in Fig. S36 is 51.9 Å, longer than the layer spacing *d* value calculated by XRD (37.1 Å). Thus, the SmA phase of **Rtx12** can be classified as a double bilayer structure with interdigitated alkyl chains[57], where flexible tails penetrate into adjacent phases (Fig. S39).

Mechanism of Liquid Crystallinity in Rtx12

To identify the elements of molecular structure that enable **Rtx12** to exhibit a thermotropic LC phase, we conducted thermodynamic studies of three types of comparative compounds using DSC, POM, and VT-XRD.

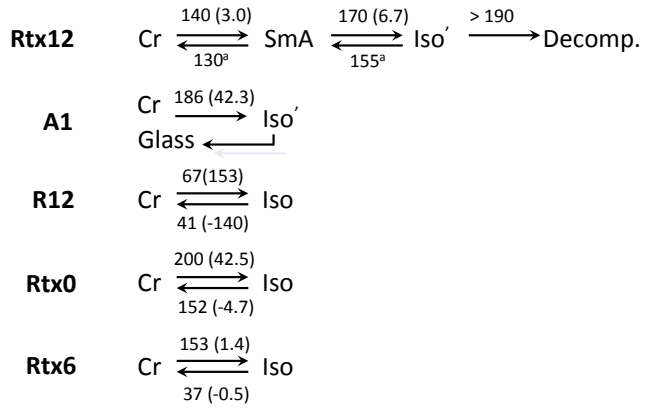

Fig. 4 Phase transition temperatures of the rotaxanes, axle, and ring in °C and their enthalpies in kJ/mol (in parentheses) based on DSC thermograms. Note the superscript of a means the estimated figure from VT-XRD results. Cr, crystalline phase; SmA, smectic A; phase; Iso, isotropic phase; Iso', thermally unstable isotropic phase; Decomp., thermal decomposition.

Firstly, we confirmed that each molecular component alone of **Rtx12**, the axle **A1**, and the ring **R12** showed no LC phase (Fig. S440–S46). Their phase transition behaviour is summarized in Fig. 4. The axle **A1**, a bare tetravalent cation, melted at 186 °C on heating, accompanied by partial decomposition, and then was vitrified upon cooling. **R12** exhibited a stable crystalline–isotropic phase transition upon heating and cooling. Neither molecular component of **Rtx12** exhibited an LC phase. Secondly, an equimolar mixture of **A1** and **R12** was evaluated. As confirmed by the NMR and UV–vis results, this mixture cannot form a rotaxane structure due to the bulky end stoppers of **A1**; therefore, it serves as a comparison having the same chemical composition as **Rtx12** but forming no rotaxane structure. This mixture also exhibited no LC phase. Upon cooling down from isotropic temperatures, POM and XRD observations (Fig. S47–S48) suggested independent **A1** vitrification and **R12** crystallization during the cooling process. This result supports the idea that the LC nature of **Rtx12** is enabled by its rotaxane structure. Finally, to understand the role of alkyl side chains equipped with a ring in the rotaxane, we prepared two other rotaxanes for comparison: a [2]rotaxane with simple DB24C8 without any side chains (**Rtx0**)[44] and a [2]rotaxane with shorter C6 side chains (**Rtx6**). **Rtx0** melted at 203 °C due to an isotropic–crystalline phase transition and did not show any LC phases on either the heating or cooling process (Fig. S49–S50). **Rtx6** also showed no LC phase but an isotropic to crystalline phase transition at a lower temperature than **Rtx12** (Fig. S51–S52). This indicates that sufficiently long flexible tails to the mesogen core stabilize the LC phase, as in conventional rod-like LCs. It is worth noting that all rotaxanes with **A1** as the axle decreased their phase transition temperature compared to bare **A1**, realizing stable phase transitions.

Through the three types of comparative experiments, we conclude that the rotaxane structure formation of the axle and ring molecules is critical to the LC phase exhibition. In other words, the rotaxane structure acted as a joint to physically unite the mesogen core and flexible tails, separated but necessary components for the LC expression. Application of this molecular design concept to pseudo-rotaxanes without stoppers is now under consideration. The design strategy of functional rotaxanes will enable us to make the facile synthesis of complex functional molecules utilizing physical bonding.

Conclusions

We have presented a new design concept for ionic liquid crystal (iLC) molecules, utilizing [2]rotaxane structure formation. We prepared the ionic axle molecule as a mesogen core and the ring molecule as flexible tails and then synthesized [2]rotaxane by combining them. Here, we integrated the mesogen core and flexible tails via rotaxane structure. The resulting [2]rotaxane was a thermotropic LC, showing a smectic A phase. In contrast, neither the axle nor ring possessed an LC nature. In a series of evaluation of comparison samples, we found that the rotaxane structure serves as a connection spatially linking the mesogen core and flexible tails, which enables LC phase emergence. This approach could be more versatile because iLCs can be instantly

obtained by mixing axles and rings. For example, the synthesis of pseudo-rotaxane systems is currently under investigation. This approach to designing complex functional molecules based on the physical linking of relatively simple molecules through rotaxane formation will open a new pathway for designing soft-robotic and flexible electronic materials and devices.

Author Contributions

G.W. conceived and conducted all the experiments. T.K. carried out XRD studies to characterize the liquid-crystalline properties. G.W., S.N., and A.S. wrote the manuscript. S.N. and A.S. supervised the project.

Conflicts of interest

There are no conflicts to declare.

Acknowledgments

The authors acknowledge Dr. Taku Ichibayashi for the DFT calculation of liquid crystalline rotaxane. The authors also thank Materials Analysis Division, Open Facility Center for the molecular weight measurements.

References

1 J. Le Bideau, L. Viau and A. Vioux, *Chem. Soc. Rev.*, 2011, **40**, 907–925.
2 M. Armand, F. Endres, D. R. MacFarlane, H. Ohno and B. Scrosati, *Nat. Mater.*, 2009, **8**, 621–629.
3 T. Ichikawa, T. Kato and H. Ohno, *Chem. Commun.*, 2019, **55**, 8205–8214.
4 M. Galiński, A. Lewandowski and I. Stepniak, *Electrochim. Acta*, 2006, **51**, 5567–5580.
5 B. Hu, C. Debruler, Z. Rhodes and T. L. Liu, *J. Am. Chem. Soc.*, 2017, **139**, 1207–1214.
6 C. Debruler, B. Hu, J. Moss, J. Luo and T. L. Liu, *ACS Energy Lett.*, 2018, **3**, 663–668.
7 K. Goossens, K. Lava, C. W. Bielawski and K. Binnemans, *Chem. Rev.*, 2016, **116**, 4643–4807.
8 Y. Ishii, N. Matubayasi, G. Watanabe, T. Kato and H. Washizu, *Sci. Adv.*, 2021, **7**, 1–15.
9 T. Ichikawa, M. Yoshio, S. Taguchi, J. Kagimoto, H. Ohno and T. Kato, *Chem. Sci.*, 2012, **3**, 2001–2008.
10 T. Kobayashi, Y. X. Li, A. Ono, X. B. Zeng and T. Ichikawa, *Chem. Sci.*, 2019, **10**, 6245–6253.
11 B. Soberats, M. Yoshio, T. Ichikawa, X. Zeng, H. Ohno, G. Ungar and T. Kato, *J. Am. Chem. Soc.*, 2015, **137**, 13212–13215.
12 X. Qiao, P. Sun, A. Wu, N. Sun, B. Dong and L. Zheng, *Langmuir*, 2019, **35**, 1598–1605.
13 E. J. W. Goodby and P. R. P. J. Collings, T. Kato, C. Tschierske, H. Gleeson, *Wiley-VCH, Weinheim, Ger.*
14 C. M. Paleos and D. Tsiourvas, *Angew. Chem. Int. Ed.*, 1995, **34**, 1696–1711.
15 T. Kato, J. Uchida, T. Ichikawa and T. Sakamoto, *Angew. Chem. Int. Ed.*, 2018, **57**, 4355–4371.
16 I. Aprahamian, T. Yasuda, T. Ikeda, S. Saha, W. R. Dichtel, K. Isoda, T. Kato and J. F. Stoddart, *Angew. Chem. Int. Ed.*, 2007, **46**, 4675–4679.
17 M. Lehmann, M. Dechant, M. Lambov and T. Ghosh, *Acc. Chem. Res.*, 2019, **52**, 1653–1664.
18 J. Uchida, B. Soberats, M. Gupta and T. Kato, *Adv. Mater.*, 2022, **34**, 1–33.
19 J. Watanabe, M. Hayashi, Y. Nakata, T. Niori and M. Tokita, *Prog. Polym. Sci.*, 1997, **22**, 1053–1087.
20 W. S. Li, Y. Yamamoto, T. Fukushima, A. Saeki, S. Seki, S. Tagawa, H. Masunaga, S. Sasaki, M. Takata and T. Aida, *J. Am. Chem. Soc.*, 2008, **130**, 8886–8887.
21 S. Asaftei, M. Ciobanu, A. M. Lepadatu, E. Song and U. Beginn, *J. Mater. Chem.*, 2012, **22**, 14426–14437.
22 O. Cabeza, E. Rilo, L. Segade, M. Domínguez-Pérez, S. García-Garabal, D. Ausín, E. López-Lago, L. M. Varela, M. Vilas, P. Verdía and E. Tojo, *Mater. Chem. Front.*, 2018, **2**, 505–513.
23 C. Y. Chang, K. W. Ho, C. S. Hsu, C. H. Lin, S. Gauza and S. T. Wu, *Liq. Cryst.*, 2009, **36**, 425–433.
24 L. Striepe and T. Baumgartner, *Chem. Eur. J.*, 2017, **23**, 16924–16940.
25 G. Casella, V. Causin, F. Rastrelli and G. Saielli, *Phys. Chem. Chem. Phys.*, 2014, **16**, 5048–5051.
26 R. T. Wang, G. H. Lee and C. K. Lai, *CrystEngComm*, 2018, **20**, 2593–2607.
27 Y. Li, T. Liu, H. Liu, M. Z. Tian and Y. Li, *Acc. Chem. Res.*, 2014, **47**, 1186–1198.
28 H. Iguchi, H. Furutani and N. Kimizuka, *Front. Chem.*, 2021, **9**, 1–12.
29 A. K. Blackburn, A. C. H. Sue, A. K. Shveyd, D. Cao, A. Tayi, A. Narayanan, B. S. Rolczynski, J. M. Szarko, O. A. Bozdemir, R. Wakabayashi, J. A. Lehrman, B. Kahr, L. X. Chen, M. S. Nassar, S. I. Stupp and J. F. Stoddart, *J. Am. Chem. Soc.*, 2014, **136**, 17224–17235.
30 D. B. Amabilino and J. F. Stoddart, *Chem. Rev.*, 1995, **95**, 2725–2828.
31 M. Raymo, J. F. Stoddart, P. Incorporating and C. Ethers, .
32 J. F. Stoddart, *Angew. Chem. Int. Ed.*, 2017, **56**, 11094–11125.
33 S. Mena-Hernando and E. M. Pérez, *Chem. Soc. Rev.*, 2019, **48**, 5016–5032.
34 M. Xue, Y. Yang, X. Chi, X. Yan and F. Huang, *Chem. Rev.*, 2015, **115**, 7398–7501.
35 F. Saito and J. W. Bode, *Chem. Sci.*, 2017, **8**, 2878–2884.
36 Y. Sagara, M. Karman, E. Verde-Sesto, K. Matsuo, Y. Kim, N. Tamaoki and C. Weder, *J. Am. Chem. Soc.*, 2018, **140**, 1584–1587.
37 J. E. Hertzog, V. J. Maddi, L. F. Hart, B. W. Rawe, P. M. Rauscher, K. M. Herbert, E. P. Bruckner, J. J. de Pablo and S. J. Rowan, *Chem. Sci.*, 2022, 5333–5344.
38 G. Gil-Ramírez, D. A. Leigh and A. J. Stephens, *Angew. Chem. Int. Ed.*, 2015, **54**, 6110–6150.
39 R. S. Forgan, J. J. Gassensmith, D. B. Cordes, M. M. Boyle, K. J. Hartlieb, D. C. Friedman, A. M. Z. Slawin and J. F.

Stoddart, *J. Am. Chem. Soc.*, 2012, **134**, 17007–17010.

40 H. R. Wessels, C. Slebodnick and H. W. Gibson, *J. Am. Chem. Soc.*, 2018, **140**, 7358–7370.

41 Y. Jiao, L. Đorđević, H. Mao, R. M. Young, T. Jaynes, H. Chen, Y. Qiu, K. Cai, L. Zhang, X. Y. Chen, Y. Feng, M. R. Wasielewski, S. I. Stupp and J. F. Stoddart, *J. Am. Chem. Soc.*, 2021, **143**, 8000–8010.

42 S. J. Loeb, J. Tiburcio, S. J. Vella and J. A. Wisner, *Org. Biomol. Chem.*, 2006, **4**, 667–680.

43 S. J. Loeb, J. Tiburcio and S. J. Vella, *Org. Lett.*, 2005, **7**, 4923–4926.

44 D. J. Mercer, S. J. Vella, L. Guertin, N. D. Suhan, J. Tiburcio, V. N. Vukotic, J. A. Wisner and S. J. Loeb, *Eur. J. Org. Chem.*, 2011, 1763–1770.

45 N. D. Suhan, L. Allen, M. T. Gharib, E. Viljoen, S. J. Vella and S. J. Loeb, *Chem. Commun.*, 2011, **47**, 5991–5993.

46 Y. Abe, H. Okamura, S. Uchida and T. Takata, *Polym. J.*, 2014, **46**, 553–558.

47 C. C. Carmona-Vargas, L. Faour, S. Tokunaga, D. Constantin, G. Fleith, E. Moulin and N. Giuseppone, *ChemistryEurope*, 2024, **2**, e202300069, 1–5.

48 J. Terao, S. Tsuda, Y. Tanaka, K. Okoshi, T. Fujihara, Y. Tsuji and N. Kambe, *J. Am. Chem. Soc.*, 2009, **131**, 16004–16005.

49 N. D. Suhan, S. J. Loeb and S. H. Eichhorn, *J. Am. Chem. Soc.*, 2013, **135**, 400–408.

50 G. Casella, V. Causin, F. Rastrelli and G. Saielli, *Liq. Cryst.*, 2016, **43**, 1161–1173.

51 J. Sakuda, E. Hosono, M. Yoshio, T. Ichikawa, T. Matsumoto, H. Ohno, H. Zhou and T. Kato, *Adv. Funct. Mater.*, 2015, **25**, 1206–1212.

52 G. Washino, M. A. Soto, S. Wolff and M. J. MacLachlan, *Commun. Chem.*, 2022, **5**, 6–11.

53 K. J. Chen, P. L. Chen and M. Horie, *Sci. Rep.*, 2017, **7**, 1–12.

54 Y. Okumura and K. Ito, *Adv. Mater.*, 2001, **13**, 485–487.

55 Y. Nakamura, A. Asami, T. Ogawa, S. Inokuma and J. Nishimura, *J. Am. Chem. Soc.*, 2002, **124**, 4329–4335.

56 S. Zhang, K. Luo, H. Geng, H. Ni, H. Wang and Q. Li, *Dalt. Trans.*, 2017, **46**, 899–906.

57 M. Yang, K. Stappert and A. V. Mudring, *J. Mater. Chem. C*, 2014, **2**, 458–473.